FIFTH AUSTRALASIAN CONFERENCE

on

HYDRAULICS AND FLUID MECHANICS

at

University of Canterbury, Christchurch, New Zealand

1974 December 9 to December 13

SECONDARY FLOWS IN ROTATING CHANNELS

by

Mitsukiyo MURAKAMI, Dr. Professor

Kouji KIKUYAMA, Research Assistant

SUMMARY

This paper represents an experimental study on the secondary flow in rotating channels having curved passages at the entrance. Uneven distribution of velocity due to the inlet curvature causes a peculiar wavy motion governed by Coriolis forces. The maximum velocity points of the uneven flow move on a sinuous curve along the channel axis. Change of this velocity causes a secondary circulatory flow, which brings about an abnormal rise of hydraulic resistance in the rotating channel. By changing the shape of the channel cross sections, the effect on the flow was investigated. The wavy motion is much suppressed in channels having less aspect ratios.

M. Murakami, Nagoya University, Nagoya, Japan

K. Kikuyama, Nagoya University, Nagoya, Japan

Nomenclature

Ep_1= pressure energy flux, Eq. (7)
Ep_2= pressure energy flux, Eq. (8)
Ek = kinetic energy flux, Eq. (3)
L^*= representative length of channel section, Eq. (1)
L_1= dimension of the cross section of channel (A)
L_2= dimension of the cross section of channel (B)
L_3= dimension of the cross section of channel (C)
q = number of waves included in axial length of $2\pi L^*$
Vm = mean flow velocity
U_z = dimensionless axial velocity
U_x = x-component of dimensionless secondary velocity
U_y = y-component of dimensionless secondary velocity
X_o= x-coordinate of flow centre, Eq. (2)
ω = angular velocity of channel
Ω = spin ratio (= $\omega L^*/ 2Vm$)

1. Introduction

The flow in a duct rotating about an axis perpendicular to the flow direction receives Coriolis acceleration which causes deformations of velocity profiles and pressure distributions of the main flow, and results in an excessive hydraulic loss. This is a major problem in designing centrifugal pumps or water-cooled turbo-generator rotors.

Many papers on this subject have been previously published but there is little detailed experimental information because of the inherent difficulty of flow measurements. Domm[1] and Kesslitz[2] measured the distribution of pressures in the impeller, and Howard and Lennenmann[3] measured both primary and secondary velocities in centrifugal impellers and gave a short analysis on the secondary flow. Dobner[4] obtained the velocity distribution and hydraulic resistance of a rotating channel with a aquare section and discussed the effect of rotation. Johnston[5], Moore[6] and Moon[7] studied in great detail the flows in the rotating rectangular ducts experimentally and analyzed the results theoretically. Seelig[8] and Kisboskoi[9] measured the hydraulic loss of rotating channels with a circular section and found that the loss was increased by channel rotation. Ito and Nanbu[10] investigated the hydraulic resistance of a rotating channel under saturated flow conditions.

A curved passage located at the entrance of a rotating duct brings about a deformed inlet velocity, which produces a particular secondary flow in the

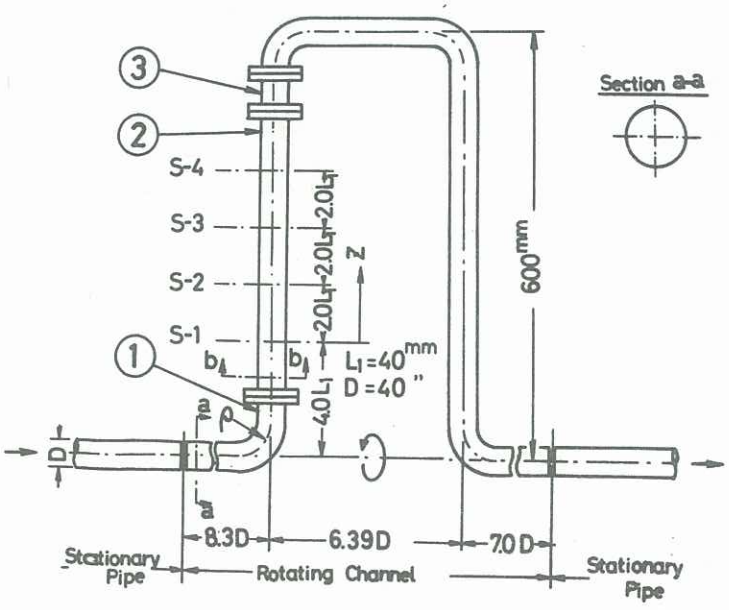

Fig. 1 Form and Dimensions of Rotating Channel

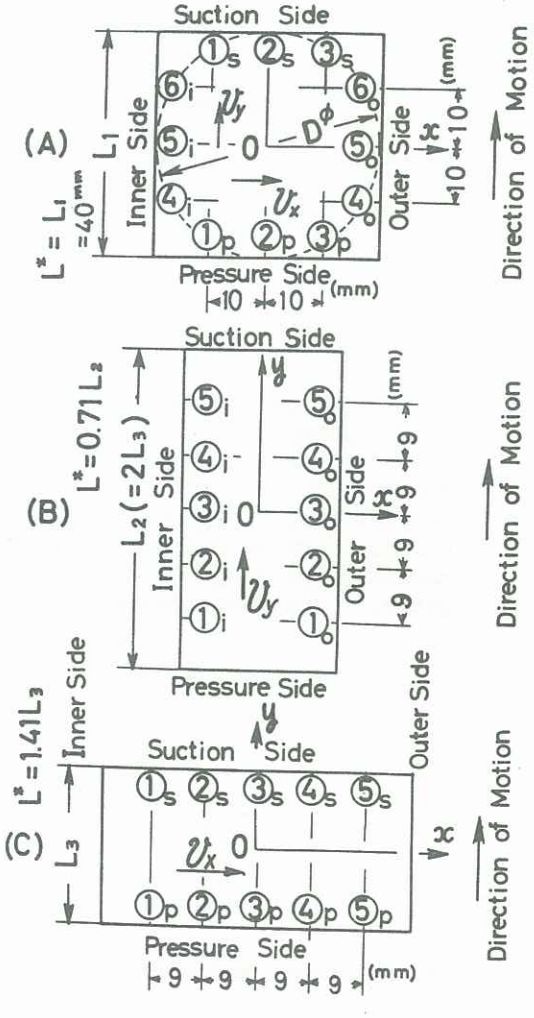

Fig. 2 Shapes of Channel Cross Section

rotating field. The maximum velocity points shift from section to section, showing a wavy locus along the channel.

The present paper describes the behaviour of this secondary flow observed in cylindrical channels of rectangular cross sections. Kurosaka[11] studied a wavy nature of flow in the laminar boundary layer of a rotating channel. The wavyness is limited only to the inlet region of the straight rotating channel, and it belongs to a different category than the flow as described in this paper. Similar kinds of wavy flow are observed in the region of stationary curved ducts.

2. Test Apparatus

A schematic outline of the experimental arrangement and detailed dimensions of the rotating channel are shown in Fig. 1. The pipe line is composed of a stationary pipe, a U-shaped rotating channel, another long stationary pipe. The rotating part was supported by two bearings and driven by a variable speed motor. To correct the flow condition, a rectifying tank was provided in the stationary pipe upstream of the test section and water was led to the rotating duct. The test sector of the rotating channel ② in Fig. 1 was replaced by ducts of rectangular cross sections, the aspect ratios of which are 1:2, 1:1, and 2:1, respectively. The periphery of the circular channel section of diameter D inscribes the square of the cross section of channel (A). Each channel has the same cross-sectional area and, hence, the ratio of linear dimensions of the sections measured in the moving direction become $L_1 : L_2 : L_3 = 1 : 1.4 : 0.707$. A cylindrical Pitot tube of 2 mm diameter was traversed along the lines indicated by $①_s$-$①_p$, $②_s$-$②_p$, ···, and $⑥_i$-$⑥_o$, at each section of rotating channel, S-1, S-2, ·····, S-4, respectively, in Figs. 1 and 2. The pressure in the rotating channel were transmitted to the stationary system through mechanical seals and the pressures were read by means of manometers.

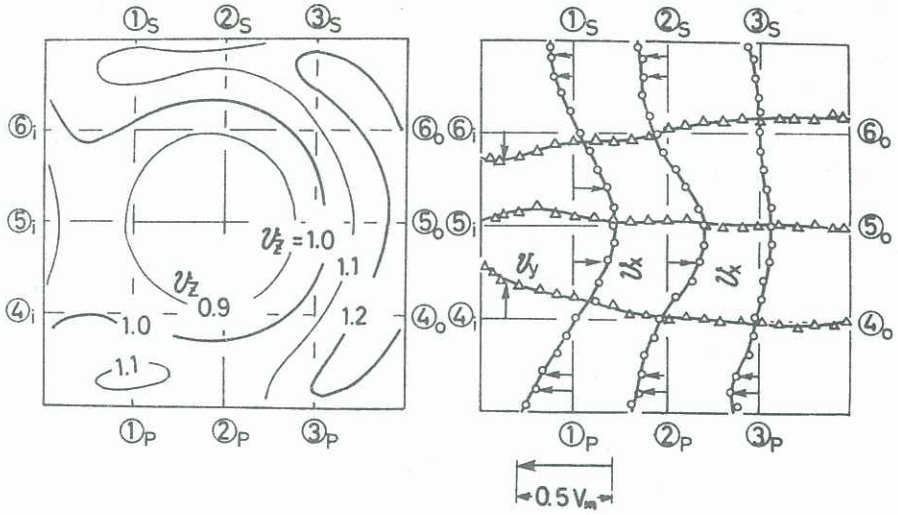

Fig. 3 Velocity Distributions at Section S-1 ($\Omega = 0$)

3. Experimental Results and Discussion

i) Channel (A) (Square Section)

The velocity distribution, including both primary and secondary velocities in channel (A) in the stationary state, is shown in Fig. 3. Distribution of velocity components v_z, v_x, and v_y are nearly in symmetry with respect to the plane of bend represented by $⑤_i$-$⑤_o$, showing the effects of the inlet bend. Rotation of the channel changes the velocity profiles. The results are shown in Fig. 4, where Ω is the spin ratio given by $\omega L^*/2V_m$, the reciprocal of which is Rossby number. The representative length in this expression is as shown in Fig. 2, namely:

$$L^* = L_1 = 0.71\,L_2 = 1.41\,L_3 \quad \cdots\cdots\cdots (1)$$

Similarity of velocity profiles is seen to be confirmed when Ω is kept constant, irrespective of Reynolds numbers and rotational speeds. The changes of velocity profiles along the channel are shown in Figs. 5(a), (b), and (c) for $\Omega = 0.5$. At section S-1 high velocities are displaced from the channel axis toward the suction side ($①_s$-$②_s$-$③_s$), where the pressure is lowered by the Coriolis force. The high velocity near the outer wall $⑥_o$ will be due to the curved motion of water in the inlet bend, and another high velocity

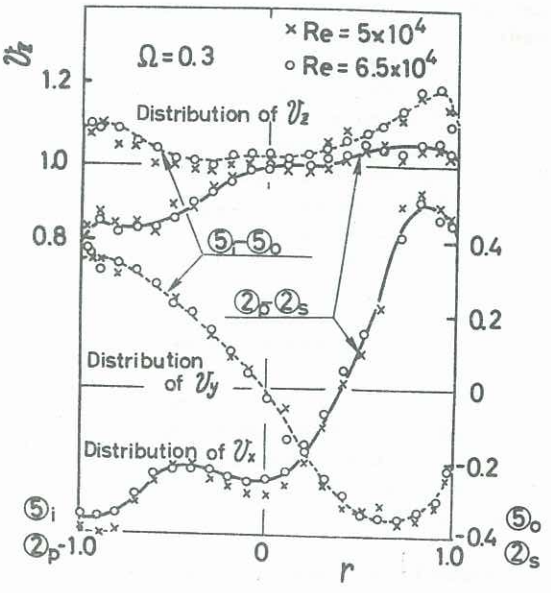

Fig. 4 Similarity of Velocity Profiles ($\Omega = 0.3$)

near the inner wall ⑥$_i$ will be caused by the accelaration of the Coriolis force based on the secondary flow velocity as described later. The Coriolis force based on the primary velocity acts on the direction perpendicular to U_Z so as to elevate the pressure on the wall in the direction of rotation and to decrease the pressure on the opposite wall.

The change of wall pressure is intensified in the high velcity region. If some deformation of flow pattern is initially given, the Coriolis force based on the deformed velocity produces unbalanced pressures on the channel wall, and a secondary circulating flow will be developed.

Thus, the shifted higher velocities in section S-1, just after the inlet bend, will call forth a clockwise component of secondary circulating flow U_Y as shown in Fig. 5. Coupled with the velocity of channel ω, this secondary flow gives rise to another Coriolis force $F_Y = -2\rho\omega U_Y$, which acts parallel to the channel axis. The sign of the velocity component U_Y is negative in the outer part of the section and positive in the inner part. The force accelerates the slower moving water near the inner wall and decelerate the faster moving water in the outer region. Resulting flow pattern in section S-2 is nearly opposite to the flow patterns observed in section S-1. This newly constructed, uneven velocity at section S-2 causes again unbalanced pressure rise on the channel wall and a counterclockwise secondary circulating flow begins to grow. This secondary flow again shifts the high velocity point to the outer region as is seen in section S-3. These phenomena are repeated downstream and, thus, the position of maximum velocities is changed alternatively along the channel, displaying wavy pattern of flow as seen in Fig. 5.

ii) Channel (B) (Rectangular Section with Aspect Ratio of 1:2)

The longer side of the cross section is in the

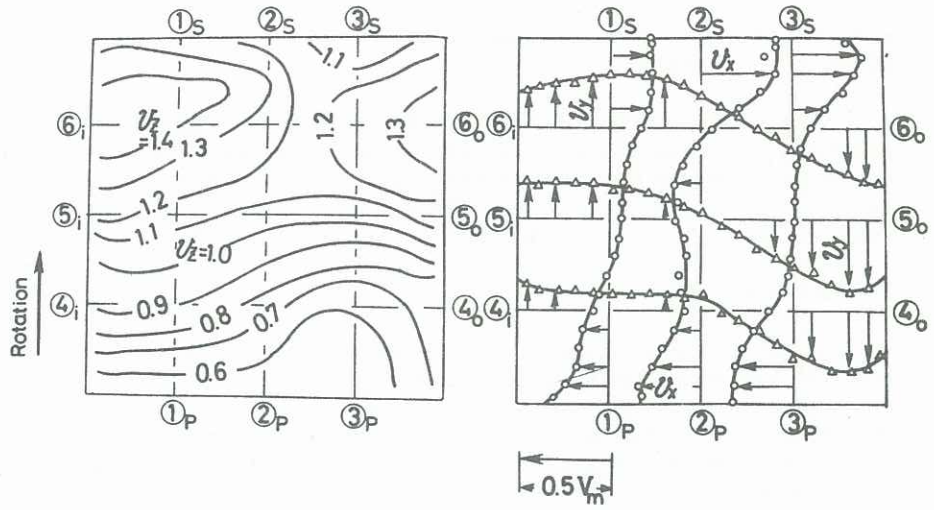

(a) Section S-1

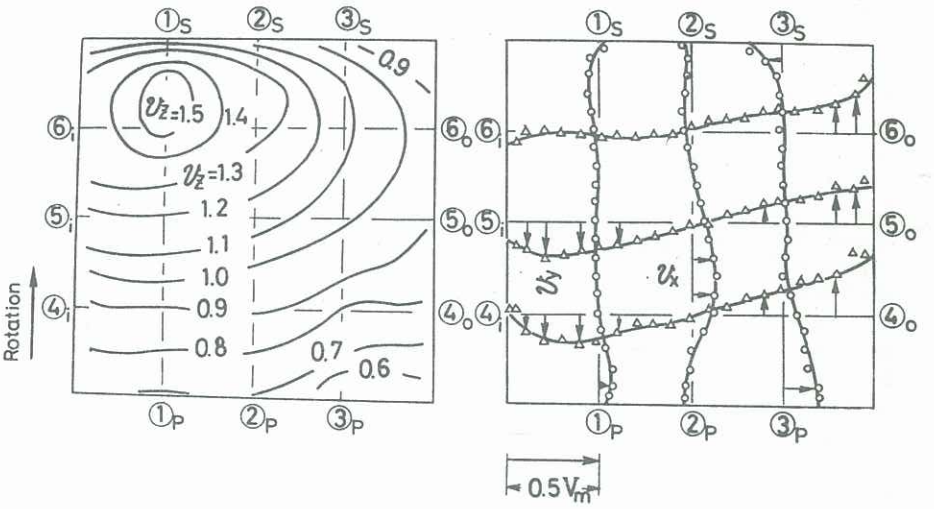

(b) Section S-2

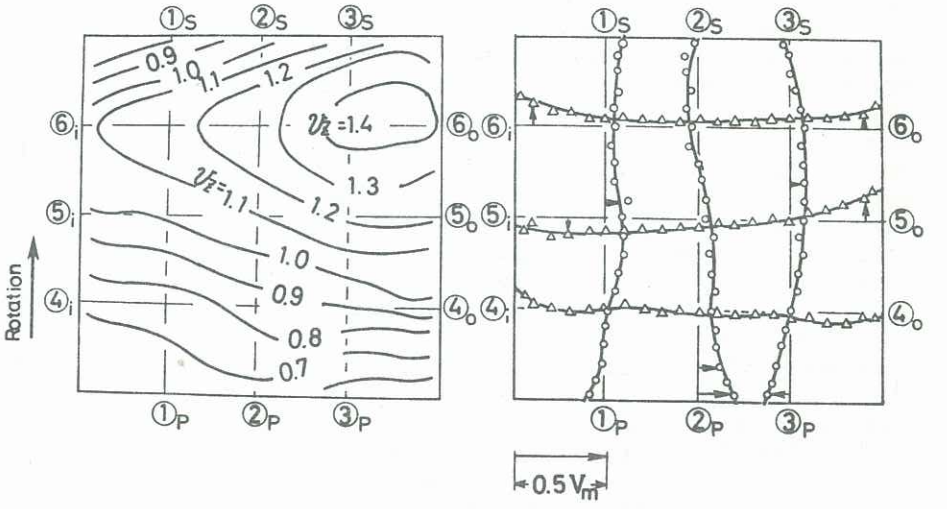

(c) Section S-3

Fig. 5 Velocity Distributions in Channel (A) (Ω = 0.5)

direction of motion as in the impeller channels of a centrifugal pump. When the channel is held stationary, the velocity distributions, both primary and secondary, are symmetrical to the plane of bend represented by $③_i$- $③_o$ in Fig. 2(B). Change of velocity distributions due to rotation is illustrated in Figs. 6(a), (b), and (c), when Ω = 0.42. The main axial flow is shifted to the low pressure side at section S-1, and a clockwise secondary flow v_y is produced by the Coriolis acceleration due to the mainflow. In this case an alternative change of the velocity distributions along the channel is hardly seen, but when $\Omega >$ 0.57, it is visible within a limited range. This will probably be due to a strong damping action on the wavy motion. The uneven main flow velocity recovers its uniformity rapidly.

iii) Channel (C) (Rectangular Section with Aspect Ratio of 2:1)

Figures 7(a), (b), and (c) show the velocity distributions when the channel was rotated at the rate of Ω = 0.56. At section S-1 the maximum axial velocity point is found near the inner wall ($①_s$) and a strong clockwise secondary flow can be seen. At section S-2, however, the sense of the secondary flow is reversed and at section S-3 the maximum flow velocity is displaced toward the outer side of channel ($⑤_s$). The wavy change of velocity distribution in this channel is more remarkable than in channel (B), showing less damping action.

iv) Centre of Momentum Flux

To investigate the longitudinal change of the axial velocity distributions the centre of the momentum flux through a section is employed as expressed by

$$X_o = \int_{-1}^{1}\int_{-1}^{1} v_z\, x\, dx\, dy \quad \ldots\ldots(2)$$

where x is the dimensionless expression of X-coordinate as in Fig. 2. The value of X_o for the channels of rectangular cross section is plotted in Figs. 8. In channel (B) the wavyness of X_o is only visible when the spin ratio Ω exceeds 0.57, but in channel (C) the wavyness appears at much lower values of Ω . With the results in Fig. 8 the relationship between the spin ratio Ω and the number of waves g included in the axial length of $Z = 2\pi L^*$ can be derived as in Fig. 9. The result is approximately expressed by $g = 2\Omega$, which is independent of the shape of the channel sections.

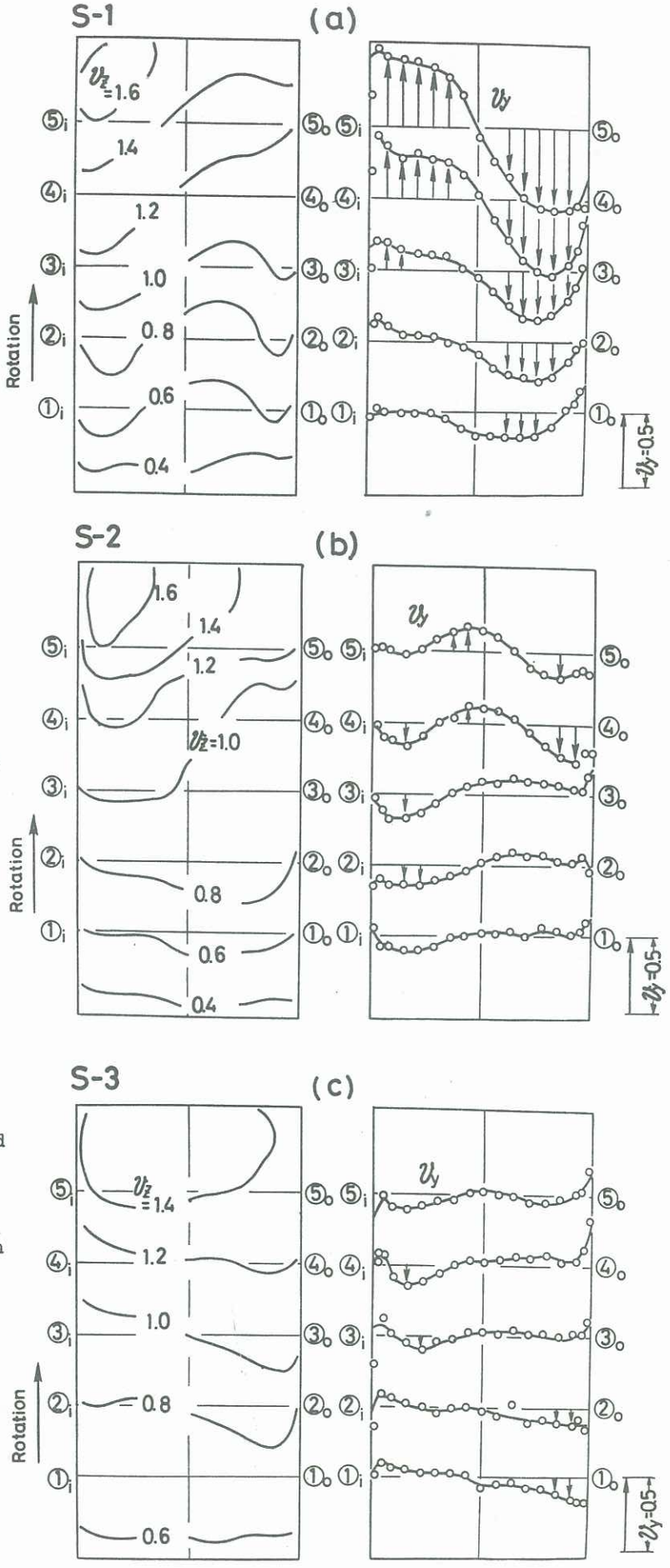

Fig. 6 Velocity Distributions in Channel (B) (Ω = 0.42)

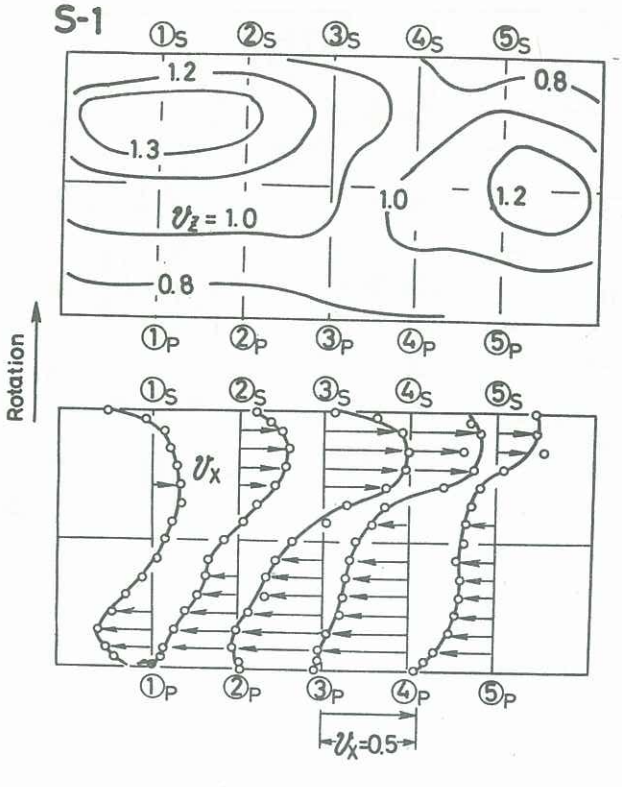

(a) Section S-1

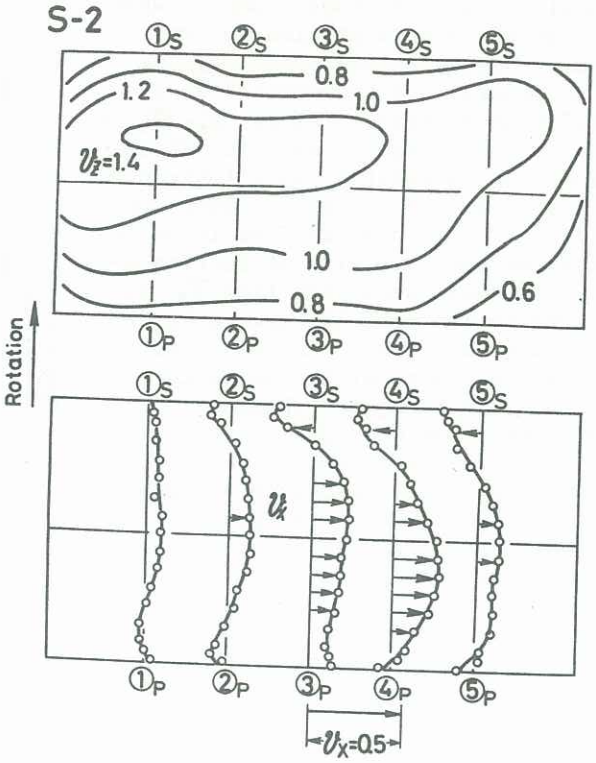

(b) Section S-2

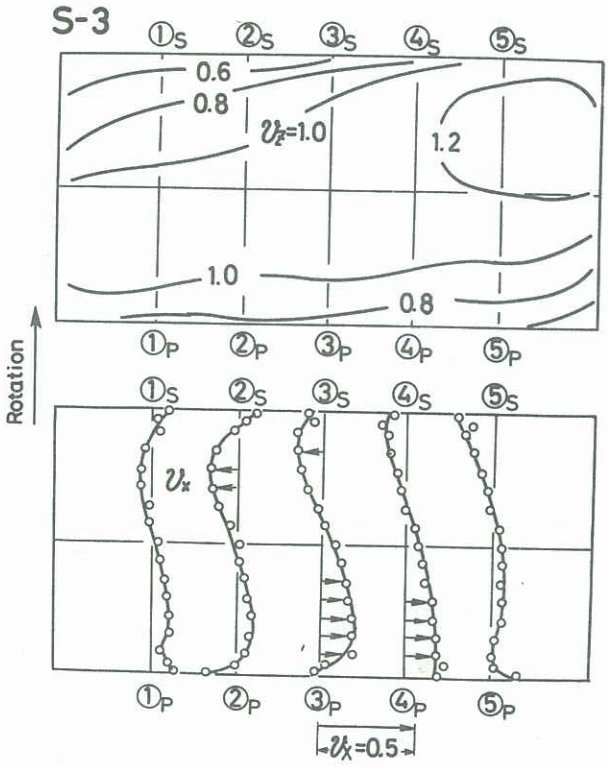

(c) Section S-3

Fig. 7 Velocity Distribution in Channel (C)
(Ω = 0.56)

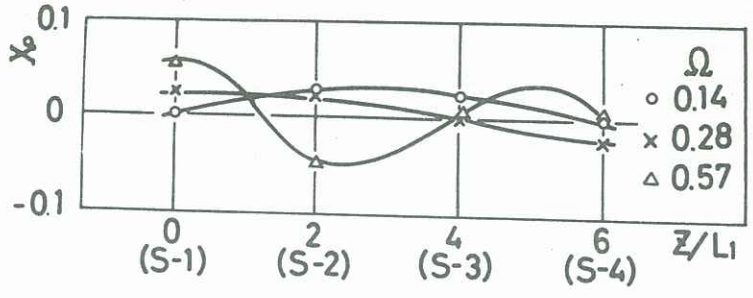

Channel (B)

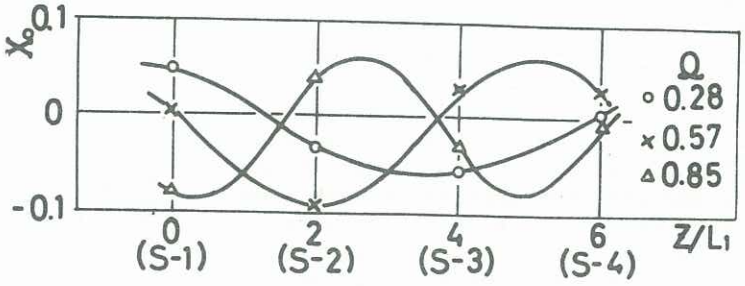

Channel (C)

Fig. 8 Changes of Flow Centre along Channel

v) Pressure and Kinetic Energies

Dimensionless expression of flow of kinetic and pressure energies per unit time across a channel section is given by

$$E_K = \int_{-1}^{1}\int_{-1}^{1} V^2 V_z \, dx\,dy \qquad \cdots\cdots\cdots (3)$$

$$E_P = \iint_{S_0} \left\{ \left(\frac{P}{\gamma}\right) V_z \Big/ \left(\frac{V_m^2}{2g}\right) S_0 \right\} dS \qquad \cdots\cdots\cdots (4)$$

where S_0 is the cross-sectional area of the channel, and P is the pressure corrected for the centrifugal effects of channel rotation. Due to the effects of the Coriolis force, the pressure P is not uniform across a channel section, and if it is referred to the pressure at the centre of each section P_0, the pressure at any point is expressed by

$$P = P_0 - (\gamma/g)\int_0^{y'} 2\omega V_z V_m \, dy' \qquad \cdots\cdots\cdots (5)$$

Substitution of Eq. (5) into Eq. (4) gives

$$E_P = E_{P1} + E_{P2} \qquad \cdots\cdots\cdots (6)$$

where

$$E_{P1} = \frac{(P_0/\gamma)}{(V_m^2/2g)} \qquad \cdots (7)$$

$$E_{P2} = -\Omega\int_{-1}^{1}\int_{-1}^{1}\left(\int_0^y V_z dy\right) V_z \, dx\,dy \qquad \cdots (8)$$

In this expression y denotes a dimensionless expression of y-coordinate. For channel (A) the pressure P_0 at the channel centre is confirmed by experiments to be nearly equal to the pressures at points ⑤$_0$ and ⑤$_i$ on the wall. The averaged value is employed for P_0:

$$P_0 = \frac{(P_{5i} + P_{50})}{2} \qquad \cdots (9)$$

Thus, the change of the pressure P_0 along the rotating channel can be estimated. Figure 10 shows the difference of the pressure energies between sections S-1 and S-4 of channel (A), ΔE_{P1}. The value of ΔE_{P1} does not exactly exhibit a hydraulic loss, but it still may be considered to roughly represent the loss. The loss begins to increase when Ω exceeds 0.2 and a noticeable effect of rotation appears on flow.

The flux of the pressure energy E_{P2} due to the Coriolis force for each section of the channel is shown in Fig. 11. The value of E_{P2} increases

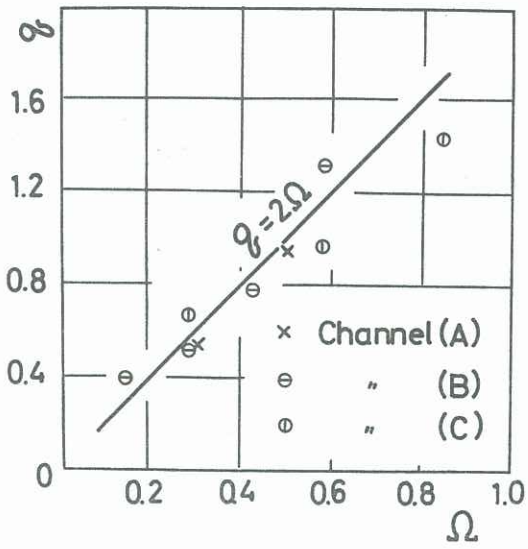

Fig. 9 Relation between q and

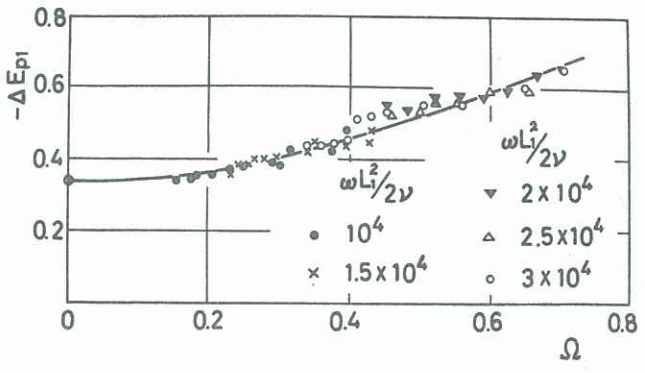

Fig. 10 Pressure Energy Loss due to Rotation

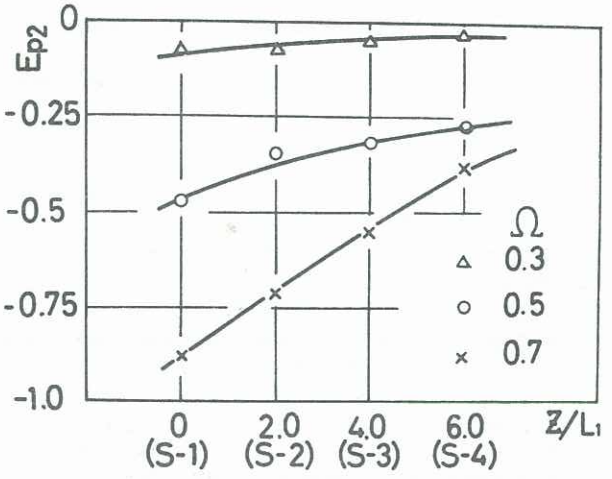

Fig. 11 Variation of Pressure Energy Flux (Channel (A))

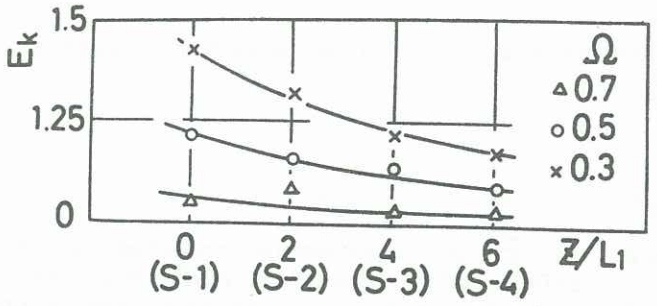

Fig. 12 Variation of Kinetic Energy Flux (Channel (A))

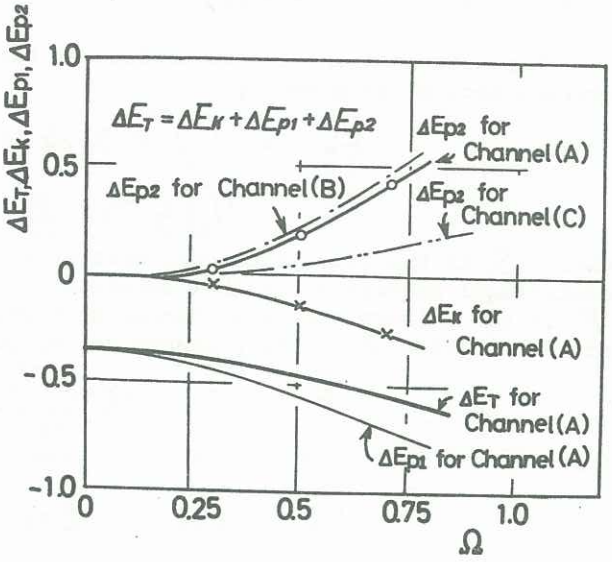

Fig. 13 Change of Energy Flux due to Rotation

downstream along the channel, because the water particles having higher velocities are shifted by secondary flow to the region of higher pressure. Figure 12 shows the kinetic energy flux E_K and it is seen to decrease downstream. This means gradual flattening of velocity profiles in the course of flow. Rate of change of E_K along the channel is increased with Ω. The total energy flux is given as the sum of each energy described above:

$$E_T = E_K + E_{p1} + E_{p2} \quad \cdots\cdots\cdots\cdots\cdots\cdots (10)$$

To examine the change of energy flux along the channel, the difference of energy fluxes between sections S-1 and S-4 is calculated by

$$(E_T)_{S-4} - (E_T)_{S-1} = \left\{(E_K)_{S-4} - (E_K)_{S-1}\right\} + \left\{(E_{p1})_{S-4} - (E_{p1})_{S-1}\right\} + \left\{(E_{p2})_{S-4} - (E_{p2})_{S-1}\right\}$$

Namely: $$\Delta E_T = \Delta E_K + \Delta E_{p1} + \Delta E_{p2} \quad \cdots\cdots\cdots\cdots\cdots\cdots (11)$$

The results are illustrated against Ω in Fig. 13. The positive value of ΔE_{p2} and the negative values of ΔE_{p1} and ΔE_K will be expected from the foregoing results. The total energy flux E_T reduces downstream but the rate is always less than that of the pressure energy flux E_{p1}. The results for channels (B) and (C) are also shown in Fig. 13. Rate of increase of ΔE_{p2} in channel (B) exceeds that of ΔE_{p2} in channel (C).

4. Conclusion

(i) Uneven distribution of primary velocities due to the inlet curvature of a rotating channel causes a Coriolis force to produce a circulating secondary flow. The secondary flow produces again another Coriolis force which acts to change the velocity distribution of the primary flow. The mutual effects of the Coriolis forces cause a wavy pattern of flow along the rotating channel.

(ii) The wavy motion is quite suppressed in channels having small aspect ratios.

(iii) The loss of flow energies in the rotating channel is increased with the spin ratio Ω.

5. Reference

(1) Domm, U. and Hergt, P., A.V.A. Göttingen, 63-01(1963), 138.
(2) Kesslitz, H. P. L., Diss. Tech. Hochschule Graz, (1959).
(3) Howard, J. H. G., and Lennenmann, E., Trans. ASME, Ser. A, 93-1(1971), 126.
(4) Dobner, E., Diss. Tech. Hochschule, Darmstatt, (1959).
(5) Johnston, J. P., Halleen, R. M., and Lezius, D. K., J. Fluid Mech., 56(1972), 533.
(6) Moore, J., M.I.T. Gas Turbine Lab. Report, 89(1967).
(7) Moon, I. M., M.I.T. Gas Turbine Lab. Report, 74(1964).
(8) Seelig, W., Verhandlungen Intern. Kongress für tech. Mech., 1(1930), 102.
(9) Kisboskoi, L., Acta. tech. hung., 22(1958), 121.
(10) Ito, H., and Nanbu, K., Trans. ASME, Ser. D, 93(1971), 383.
(11) Kurosaka, M., Trans. ASME, Ser. I, 95-1(1973), 68.